Journal Pre-proof

A digital approach to automatically assess the machining-induced microstructural surface integrity

Andrea la Monaca (Conceptualization) (Methodology) (Software) (Investigation) (Validation) (Formal analysis) (Data curation) (Writing - original draft), Zhirong Liao (Methodology) (Investigation) (Validation) (Formal analysis) (Supervision), Dragos Axinte (Conceptualization) (Investigation) (Formal analysis) (Writing - review and editing) (Supervision)

Please cite this article as: la Monaca A, Liao Z, Axinte D, A digital approach to automatically assess the machining-induced microstructural surface integrity, *Journal of Materials Processing Tech.* (2020), doi: https://doi.org/10.1016/j.jmatprotec.2020.116703

This is a PDF file of an article that has undergone enhancements after acceptance, such as the addition of a cover page and metadata, and formatting for readability, but it is not yet the definitive version of record. This version will undergo additional copyediting, typesetting and review before it is published in its final form, but we are providing this version to give early visibility of the article. Please note that, during the production process, errors may be discovered which could affect the content, and all legal disclaimers that apply to the journal pertain.
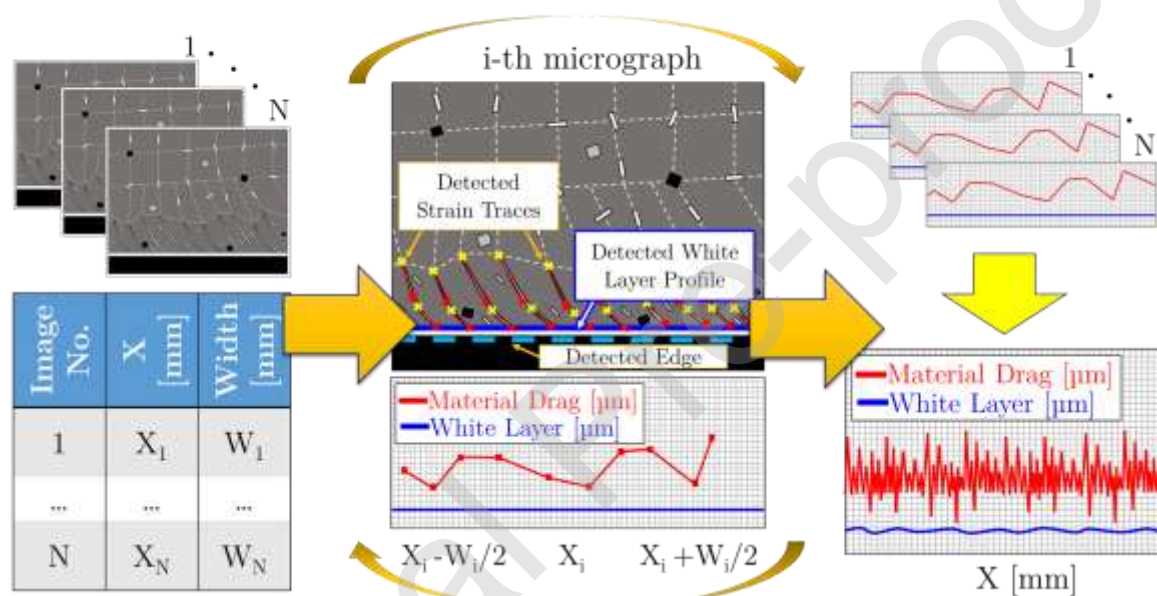
A digital approach to automatically assess the machining-induced microstructural surface integrity

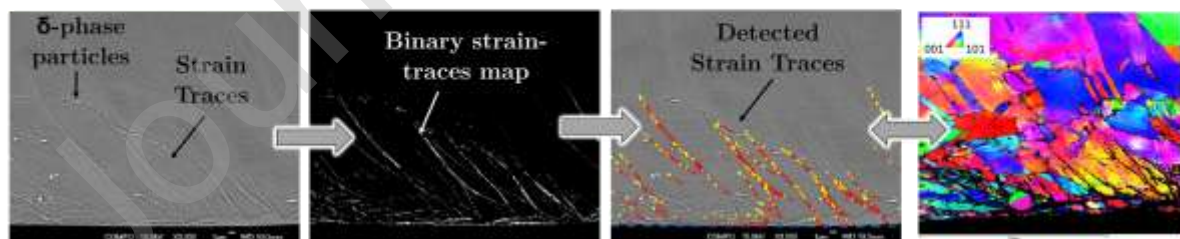Andrea la Monaca [a], Zhirong Liao [a], Dragos Axinte [a,*]

[a] Rolls-Royce University Technology Centre (UTC) in Manufacturing and On-Wing Technology, Faculty of Engineering, University of Nottingham, Nottingham, UK

Graphical Abstract

*   Corresponding   Author.
E-mail address: Dragos.Axinte@nottingham.ac.uk (D. Axinte).

HIGHLIGHTS
- Digital assessment of machining-induced microstructural surface integrity
- Detection of strain traces and white layer
- EBSD for in-depth material analysis
- System automation and processing of large material regions

Abstract

When it comes to advanced materials for safety-critical applications, the evaluation of the machining-induced microstructural surface integrity represents a primary aspect within the assessment of part quality. Nowadays, presence and extent of machining-induced microstructural anomalies in the workpiece subsurface is manually measured by human inspection of digital micrographs. In the present work, computer-based performance of this task is achieved through a set of algorithms designed to automatically identify microstructural anomalies resulting from material removal operations. Digital surface integrity assessment has been demonstrated with application to scanning electron micrographs exhibiting different levels of microstructural deformation and obtained under different imaging conditions. Furthermore, the digitally detected material condition has been investigated with the support of in-depth field emission gun scanning electron microscopy (FEG-SEM) and electron backscatter diffraction (EBSD) analysis. This has allowed the relationship between the material evidence observed through different strategies to be established. Finally, the set of algorithms has been applied to study the microstructural condition of a large material region, by performing sequential processing of a series of micrographs. In this way, the measurement procedure has been calibrated and its capability to perform surface-integrity evaluation on large areas in an automated and standardised way has been demonstrated.

1 Introduction

To ensure long lasting operation of safety-critical mechanical systems, engineers design components that must be able to safely withstand the loading conditions that develop during operation. Adequate material selection is one of the aspects that play a pivotal role to ensure part functionality and resistance over time. As a matter of fact, the continuous effort focussed on the development of increasingly high-performance materials is one of the driving research trends in aerospace (Zhang et al., 2018),

nuclear and power generation fields (Hosemann et al., 2018). However, components having identical geometry and made of the same material can exhibit profoundly different mechanical and thermal performance, depending on the way they have been processed. Many aspects of macroscopic materials behaviour are governed and explained by micro-scale physical properties generated within the material manufacturing route. Thus, when it comes to the production of safety-critical components (e.g. turbine discs of aero-engines), assessing the resulting microstructural material integrity plays an essential aspect in defining part quality and acceptability. Therefore, understanding the genesis of process-induced material alterations is of global interest for manufacturing technologists and materials designers dealing with a wide range of different operations. Examples of these are wire electrical discharge machining (Zhang et al., 2019), friction stir welding (Singh et al., 2020), deep hole drilling (Zhang et al., 2017), or laser-assisted machining (Shang et al., 2019). As reported by Kappmeyer et al. (2012), machining represents for many high-value manufacturing products one of the most demanding operations in terms of costs and process complexity. Namely, when performing material removal through chip formation, severe thermo-mechanical gradients can be generated in a confined material volume. As a consequence, remarkable material modifications could be induced in the proximity of the generated surface, which must be adequately monitored when manufacturing high-value safety-critical components, such as the ones belonging to hot sections of gas-turbine aero-engines (Hardy et al., 2014). To indicate the material condition in the proximity of a machined surface, specialists refer to the concept of microstructural Surface Integrity (SI) (Liao et al., 2019a).

Many researchers have identified how machining-induced anomalies are accountable for significant reductions in performance of advanced materials (M'Saoubi; et al., 2015). Connolley et al. (2004) have shown how broaching operations can generate severely deformed material layers responsible of reduced high-temperature fatigue behaviour of Inconel 718 specimens. Herbert et al. (2014) studied the effect of material drag and white layer generated in RR1000 as a result of hole-making processes, showing how the presence of machining-induced white layer promoted crack nucleation and propagation because of its reduced ductility. Liao et al. (2019) reported on the fundamental mechanisms of white layer formation in a new generation nickel-base superalloy, investigating the key phenomena governing the mechanical behaviour of this material region. Several studies have reported on the detrimental effect on material performance caused by the presence of microstructural anomalies induced by severe machining conditions, e.g. investigating the effects of with-etching layers (Wusatowska-Sarnek et al., 2011) and surface topography (Novovic et al., 2004) on fatigue life and crack nucleation. Therefore, investigating and characterising the microstructural surface integrity of advanced materials represents a topic of high relevance for safety critical applications such as aerospace propulsion systems or nuclear components (Gavalda Diaz et al., 2019).

An informed review on the state-of-the-art in machining-induced surface integrity evaluation for advanced alloys has been presented by Thakur and Gangopadhyay (2016). Light microscopy enables observation of surficial machining irregularities such as cracks, burrs or voids due to tool-workpiece interaction. The analysis of representative etched surfaces enables the observation of microstructural

modifications resulting from the material removal operation. When high-magnification is required, scanning electron microscopy (SEM) or field emission gun SEM (FEG-SEM) is employed to investigate small-size features. X-ray Diffraction (XRD) is one of the most adopted methods to quantify process-induced residual stresses (Arunachalam et al., 2004). Advanced techniques such as micro and nano-indentation or Electron Backscatter Diffraction (EBSD) are adopted for advanced in-situ evaluation of material hardening and plastic deformation induced in the specimen subsurface (Liao et al., 2018). When investigating the integrity of machined components, the presence of severe plastic deformation (SPD) is recognised by identifying critical microstructural indicators such as presence of material drag and/or white-etching layer in the proximity of the generated surface (M'Saoubi et al., 2014). Therefore, the identification, location and quantification of such features is mandatory to assess the levels of workpiece microstructural surface integrity (Herbert et al., 2012).

In-depth investigation on the material subsurface condition requires advanced understanding of the material deformation mechanisms and its relationship to the process-induced microstructure, which is supported by the adoption of advanced material analysis techniques as the ones previously cited. Nevertheless, surface integrity assessment is nowadays still characterized by a certain level of subjectivity and user-dependency, relying in some extent on human judgment for quantification of surface microstructural deformation. Namely, this can be particularly significant for applications involving manual assessment of material drag extent or white layer thickness from representative micrographs displaying the workpiece sub-surface condition. Manual measurements are likely to be affected by a more pronounced lack of repeatability and less robust judgement parameters, if compared with ones carried out by automated systems. In the context of microscopy, significant attention has been focused over the years on strategies to automate material analysis through digital algorithms for microstructural characterisation. Campbell et al. (2018) presented a method for automatic quantification of microstructural features such as grain size, volume fraction of globular alpha phase and alpha lath colonies size in Ti-6Al-4V. Implementing an image processing strategy based on segmentation techniques, this work demonstrated how automated approaches enable improved measurement speed and repeatability with respect to manual procedures. In the context digital characterisation of titanium alloys, Collins et al. (2009) presented a set of stereological procedures for quantification of microstructural features from SEM micrographs. Digital image processing was applied also by Yang and Liu (2016) to analyse the workpiece subsurface obtained when milling Ti-6Al-4V in terms of phase content and grain size. Zhao et al. (2019) proposed an automatic approach for measurement of grinding-induced white layer in titanium alloys. Peregrina-Barreto et al. (2013) et al. employed digital algorithms to perform grain size measurements on low carbon steel AISI 1010. Three-dimensional reconstruction techniques have been applied by Gillibert and Jeulin (2013) to analyse fragmented grains in composites. Digital image analysis has also been applied to evaluate the delamination occurring when drilling composite laminates (Davim et al., 2007). In a wider perspective, digital image processing techniques are rapidly finding an increasing number of applications in

several research fields such as biology (Lu et al., 2016), physics (Bock et al., 1995) or nano-engineering (Sajedian et al., 2019).

Digital image processing algorithms represent a route of development for several scientific applications, demonstrating possibility of measurement automation through feature detection with good levels of speed and repeatability. With regards to microstructural material characterisation, further development is possible through combination of emerging digital sciences with advanced material knowledge. When it comes to surface integrity evaluation, state-of-the-art strategies still strongly rely on manual measurement and human judgment. This specifically applies to the detection, location and quantification of process-induced microstructural anomalies in the form of material drag, which represents a key element to evaluate the microstructural integrity of surfaces generated through mechanical machining. However, inspection and detection of material drag from etched surfaces still involves significant challenges. In the first place, material drag in the form of strain traces in etched surfaces provides a visual indication of a much more complex material condition, which is not easy to judge with conventional techniques. For this reason, it is mandatory for the assessment process to be carried out by experienced users. Moreover, as the appearance of strain-traces is geometrically complex, being such entities not a continuous material feature, punctual strategies are required for effective digital detection. Therefore, standard filtering techniques are not sufficient to reliably perform this task. Moreover, because of the complexity of the material state under consideration, for the digital detection of these features to be consistent, a validation step involving in-depth material analysis is essential to confidently comprehend the visually and digitally detected indications of material deformation. These factors namely make the assessment of drag levels in machined surfaces a complicated task, which can result time consuming and repetitive from a practical point of view. Furthermore, this process needs to be carried out with high levels of repeatability and awareness, to correctly interpret the microstructural condition under observation from the material perspective. In this regards, implementation of feature-oriented digital approaches accompanied by in-depth material validation offer a promising way of bridging the existing gap. In addition to the measurement of material drag, an informed assessment of the microstructural condition of machined surfaces needs to give information on the presence of white layer in the material subsurface. Because of its homogenous and featureless appearance, digital detection of white layer is conceptually simpler, involving less complex digital strategies and algorithm validation. In this sense, this task might be considered less scientifically-appealing. Nevertheless, white layer detection does represent an object of interest when assessing surface integrity after machining. Therefore, a collateral digital algorithm has been purposely designed and integrated with the one performing digital drag detection, enabling successful combined detection of white layer presence and extent and digital assessment of material drag. In this way, the present approach aims to provide a suitable framework to automate the measurement process, performing informed and aware digital characterisation of the microstructural condition generated in high-temperature alloys after machining.

Understanding and controlling high-value manufacturing processes in terms of workpiece microstructural condition namely represents a first-order priority to meet

the excellent quality levels that notoriously characterise the manufacture of safety-critical components for the aero-engine or nuclear industry. Moreover, it serves as a core investigation route for researchers studying the fundamental micro-mechanical phenomena involved within the complex geometrical and physical modifications taking place when processing advanced materials. However, when it comes to surface integrity, for successful and trustworthy implementation of emerging digital techniques, the analysis cannot be limited on algorithm development, but must be substantiated by in-depth material understanding. This somehow still represents a missing element when looking at the existing works in the field. Within the present research, the applicability of a digital approach for microstructural surface integrity assessment is demonstrated, discussing both the algorithm digital and conceptual development, together with its validation through contextual in-depth material investigation through FEG-SEM and EBSD analysis. In this way, each step of the innovation process is knowingly developed, ensuring consistence and coherence of future surface integrity approaches with the fundamental knowledge matured in the field.

2 Conceptual framework for micrograph digital inspection

2.1 Problem Description

When analysing the microstructural condition of machined surfaces, the volume of material affected by grain distortion and deformation is usually referred to as the drag-affected area. The term 'drag' namely refers to the generation of a deformed layer in the material subsurface, due to the mechanical action of the cutting tool that induces plasticity in the volume of material participating to the process. Therefore, microstructural evidence of this phenomenon is usually found in the form of microstructural distortion, with possibility of local modifications in the material properties. In some cases, a thin layer of highly strained material can be generated in the vicinity of the machined surface, especially under aggressive cutting conditions (Liao et al., 2019b). This is usually referred to as white-etching layer, or more simply white layer. It has been previously remarked that the manufacture of safety-critical components requires such features to be avoided or minimised (depending on the case) to guarantee acceptable levels of component quality. It is further highlighted that, since high-performance components usually require employment of high-temperature alloys, these anomalies might be even more likely to be generated because of the aggressive conditions that develop when processing such advanced materials. Significant work has been published on the study and characterization of machining-induced microstructural anomalies in aerospace superalloys. M'Saoubi et al. (2014) reported on the microstructural modifications induced by abusive drilling in Alloy 718, Waspaloy, Alloy 720Li and RR1000. Liao et al. (2018) studied the influence material composition and volume fraction of gamma prime phase on the resulting surface

integrity of advanced nickel superalloys. Zhou et al. (2012) reported on the presence of major microstructural deformation in Inconel 718 as a result of aggressive processing conditions at high cutting speeds. In this context, a schematic representation of the microstructural material condition in the vicinity of machined surfaces is represented in Figure 1, with reference to nickel-base superalloy Inconel 718. The material microstructure observable through SEM displays the γ matrix, with the presence of additional constituents such as niobium and titanium carbides, and δ-phase particles decorating the grain boundaries. In general terms, the material volume in the vicinity of the surface affected by the previously introduced microstructural anomalies has been hereby indicated as "Drag-affected Area", as reported in Figure 1. Away from the machined surface, where process-induced modifications can no longer be observed, the material microstructure can be assumed to be unmodified. This portion of material has been indicated as "Base Material".
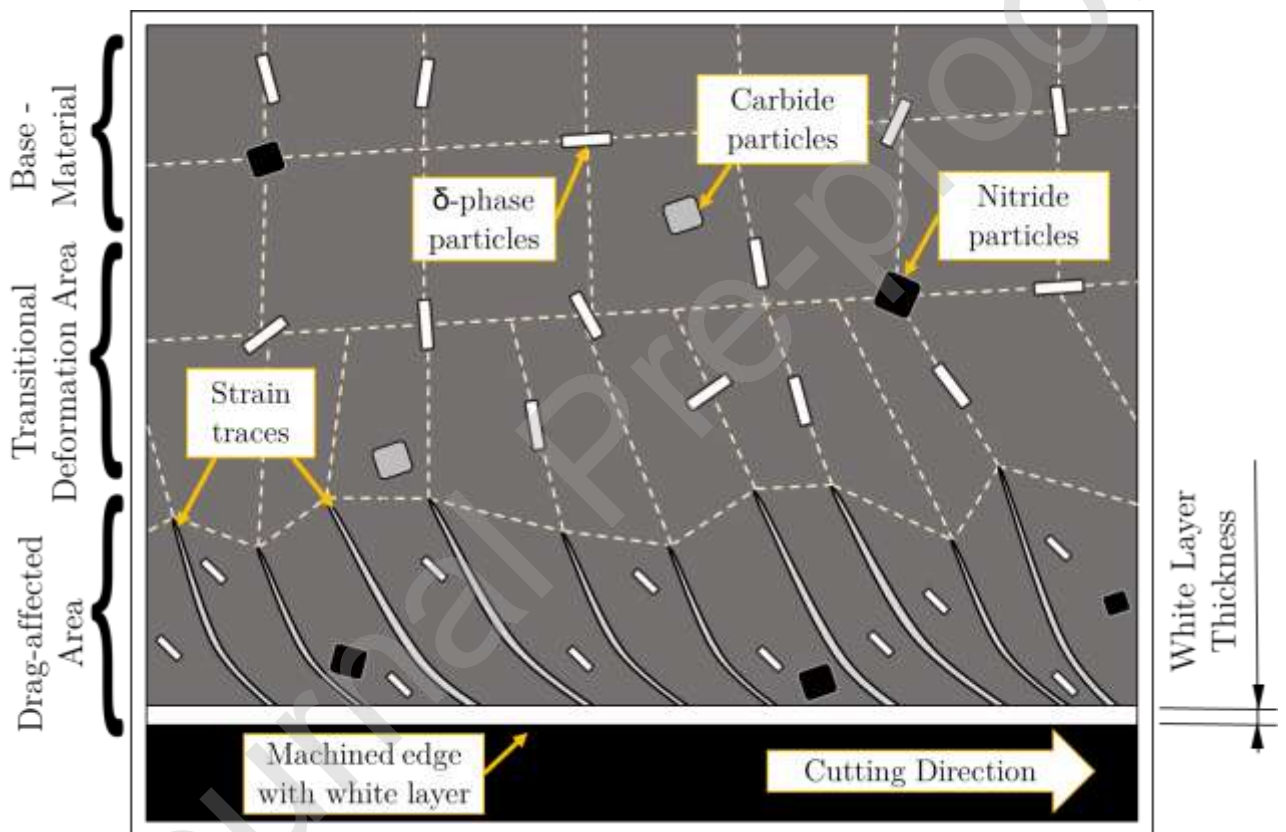

Figure 1 – Schematic representation of the typical sub-surface microstructural condition resulting from material removal through chip formation. Example represented referring to the physical metallurgy of nickel-base superalloy Inconel 718.

The severe deformation area is separated from the base material by a "Transitional Deformation Area" area, where minor microstructural modifications can occasionally be found. In order to assess the level of material deformation, the attention is focussed on the evaluation of the extent of the drag-affected area and of the presence of white layer with measurement of its thickness. Conventionally, this is carried out by manually measuring the extent of these features from visual observation of

representative micrographs. When this task is carried out by human operators, indications of microstructural alterations are inspected on relevant micrographs on a one-by-one basis. In this way, pixel-lengths measured by the user are converted to a millimetre or micron scale once a calibration reference is provided. However, manually performing this repetitive procedure on a large number of micrographs can make the process time-consuming and introduces a subjective component influencing the judgment of the observed entities.

Hence, the present work proposes an approach to leave to the computer the identification and quantification of these features, following quantitatively defined detection thresholds dictated by a material specialist. This has been successfully obtained through the development of a set of digital image processing algorithms to extract information on the material microstructure from the micrographs of interest.

2.2 Strain-traces: Detection and localisation

The digital detection of the strain traces represented in Figure 1 is carried out through a Hough-transform based algorithm. The Hough-transform is one of the most-widely used analysis techniques for the detection of edges and lines in digital images. Namely, the Hough operator allows the identification of imperfect objects whose shape belongs to a geometrical class through a voting procedure (Gonzalez et al., 2010). It is worth to mention that one of the applications of this technique in material science is Kikuchi Diffraction Patterns detection to determine lattice crystallographic orientations within EBSD mapping (Adams et al., 1993). Thus, the Hough-transform has been applied in this work for the detection of line-shaped strain traces in digital micrographs. Through this operator, a correlation is established between lines belonging to the digital image space and points of the so-called Hough-space. Nevertheless, the efficiency of a Hough-transform-based line detection algorithm depends on the quality of the input data. In Figure 1 for instance, a human observer recognises relatively quickly the presence of elongated elements, logically associating them to a series of line objects. These elements represent the geometrical entities employed by the human brain to carry out the interpretation and measurement of material drag in a given micrograph. To perform computer-based inspection however, the detection strategy must be performed through algorithmic procedures based on mathematical formulations. Subsequent logical steps are therefore required to reach the desired detection target. In this framework, with the aim of optimising the Hough-transform input quality, a (pre-filtering) function has been designed and employed to remove unnecessary digital data from the original image. This allowed the Hough-operator to be performed on a lower-level binary domain, as described in the next section. In the following, the steps implemented to digitally assess the levels of microstructural deformation in the sub-surface of machined specimens are discussed.

2.2.1 Binary Strain-traces map generation

The first step concerns the employment of a filtering function designed to isolate the features of interest from input digital micrographs. The objective is to generate a binary map representing only the subset of pixels identified as potential part of a strain trace. To this aim, removal of unneeded digital information is performed. The key idea is to input the greyscale range in which the strain traces are expected to appear, and then isolate them by analysing the greyscale map of the digital image. Before the actual binarization step, a preliminary identification and blackening of the delta-phase pixels is carried out. Namely, since such pixels tend to exhibit similar grayscale intensity to the ones belonging to strain traces, they act as a digital noise that lowers strain traces detectability, and are therefore removed from the dataset as represented in Figure 2 (a).
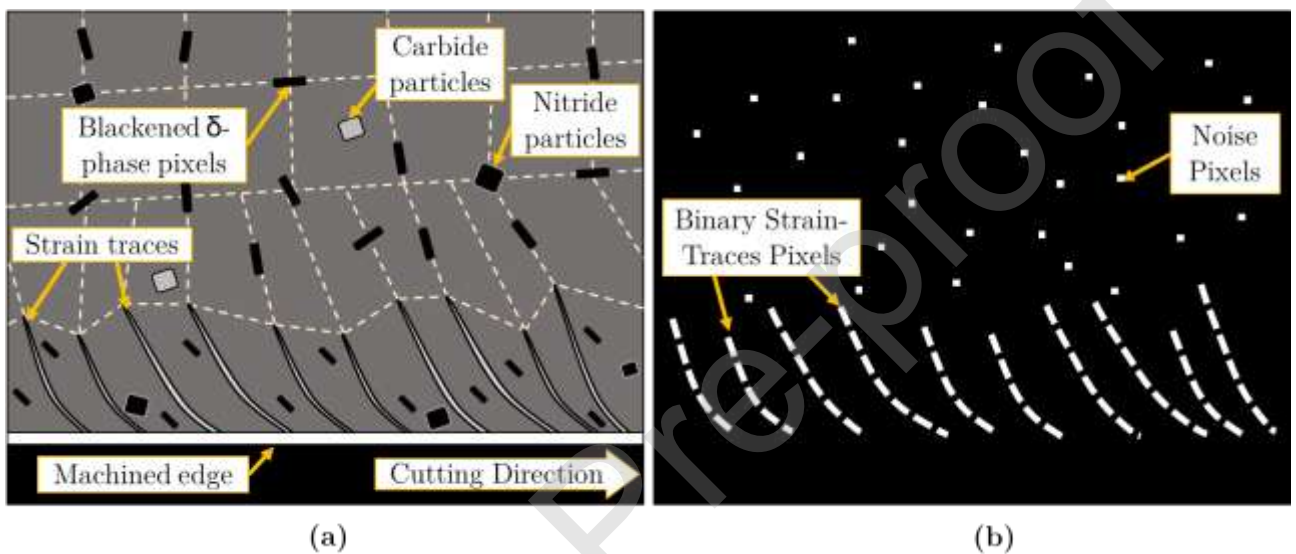

Figure 2 – Pre-processing filtering strategy. a) Removal of delta-phase pixels, b) generation of the strain traces binary map.

Subsequently, the local greyscale map and gradients are evaluated in the resulting image, to identify and discard the pixels with grayscale intensity far from a reference intensity range indicated by the user as typical of the strain-traces pixels in the imaging condition under consideration. In this way, a binary dataset representing a map with the potential strain-traces location is obtained, as shown in Figure 2 (b).

2.2.2 Strain-traces detection through Hough-transform

Within the second step, the resulting binary dataset is processed through a Hough-transform based algorithm that detects and locates the presence of lines in the input map, as shown in Figure 3(a).
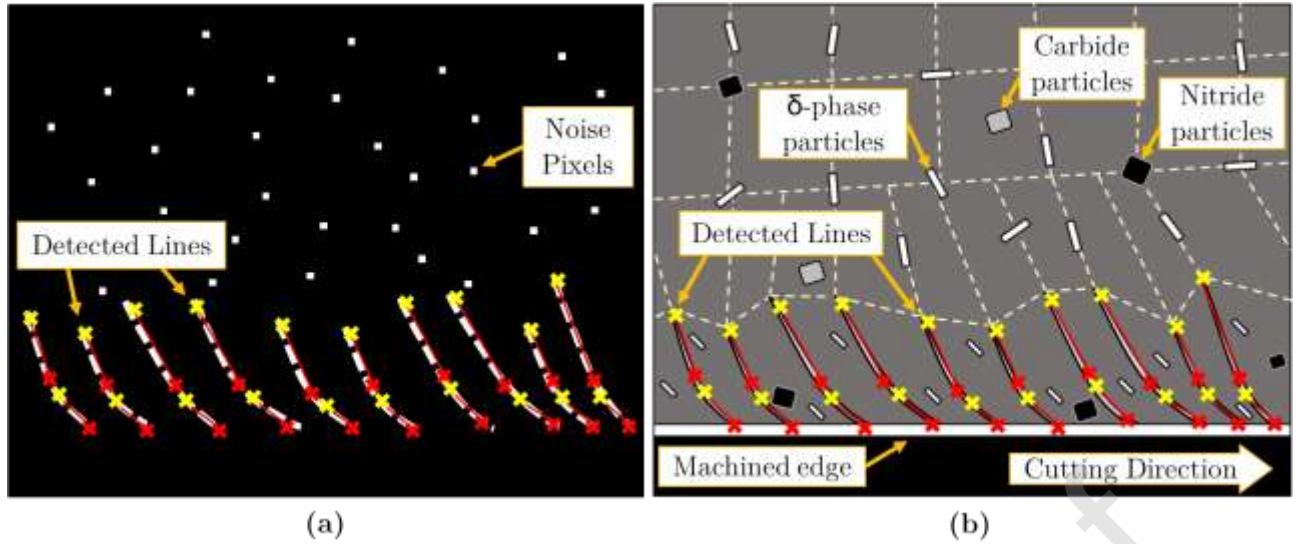
9

Figure 3 - Hough-transform based strain traces detection with detected lines (solid red line) with their upper and lower extremal points (yellow and red crosses, respectively) on binary map a) and representative micrograph b).

Once the detected Hough-lines are obtained, they are referenced to the corresponding pixel coordinates on the input digital image. This enables representation of the detected features on the original micrograph, as shown in Figure 3(b).

2.2.3 Strain-traces localization through edge-detection

At this point, the pixel coordinates of the detected lines have been obtained in the image space. In order to evaluate the extent of the material drag beneath the specimen's surface, the detected strain-traces need to be referenced to the location of the machined edge. Therefore, the third step of this algorithm was implemented to automatically detect the sample edge in the digital micrograph. The edge detection strategy also relies on a preliminary binarization procedure. This is obtained by distinguishing the pixels representing the observed material from the ones belonging to the mounting compound in which the specimen is embedded.
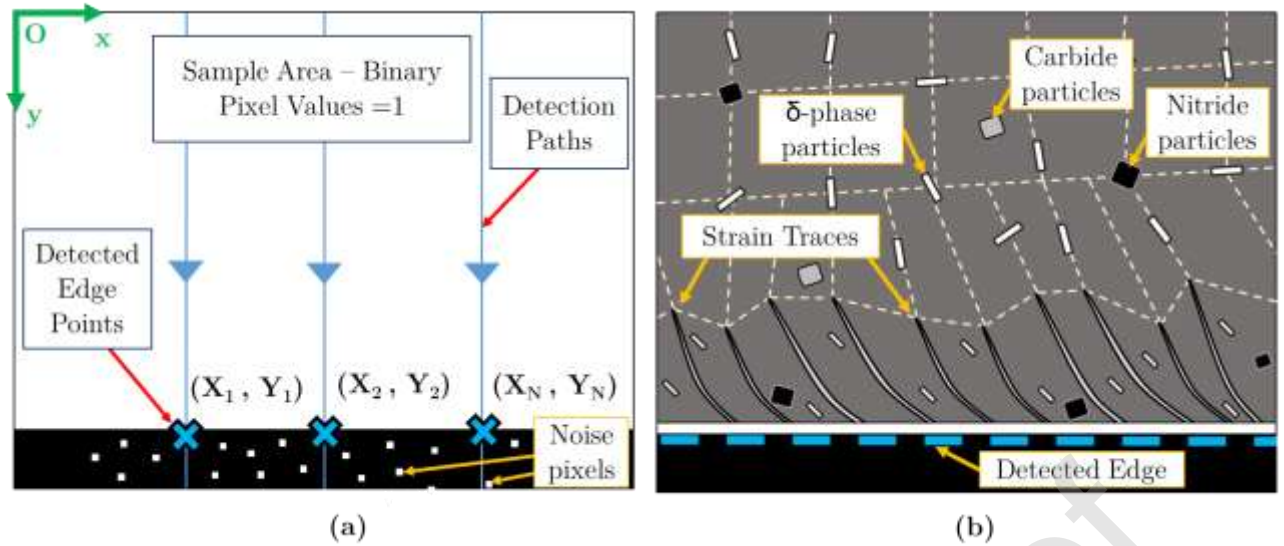
Figure 4 - Edge detection strategy. a) Schematic representation of the sample-edge recognition algorithm. b) Detected edge on representative micrograph.

The latter appears namely darker when observed by SEM, because of its lighter atomic weight. Hence, binarization is performed through a greyscale thresholding approach. Thus, the algorithm blackens pixels not satisfying a greyscale intensity condition that distinguishes pixels belonging to the observed material from ones that belong to the mounting media. Once the image is in this way binarized, vertical lines scanning is performed, as shown in Figure 4 (a). A change in binary value over a vertical line is associated with a change from material pixels to pixels representing the mounting media. Hence, the Y edge coordinate is detected for each X location, through identification of the pixel coordinate where the binary inversion occurred. Repeating this procedure on vertical lines over the whole horizontal extension of the image, the sample edge (X, Y) coordinates are successfully individuated, and can be referenced to the input micrograph as represented in Figure 4 (b). Once the edge location has been obtained, the distance between the uppermost vertexes of the detected lines - yellow cross in Figure 4(b) - and the detected edge is computed. The measurements can then be converted from pixel units to a suitable length scale, once a conversion factor is provided for the micrograph.

2.3   White Layer: Detection and Localisation

Once the presence of material drag has been digitally inspected, step 4 consists in an additional algorithm developed to detect the presence of the white layer in digital micrographs. After performing edge detection, small rectangular subsets (see inserts

11

in Fig. 5a) of the micrograph are obtained in the proximity of the machined edge, where the white layer might be present, as the one shown in Figure 5 (a).
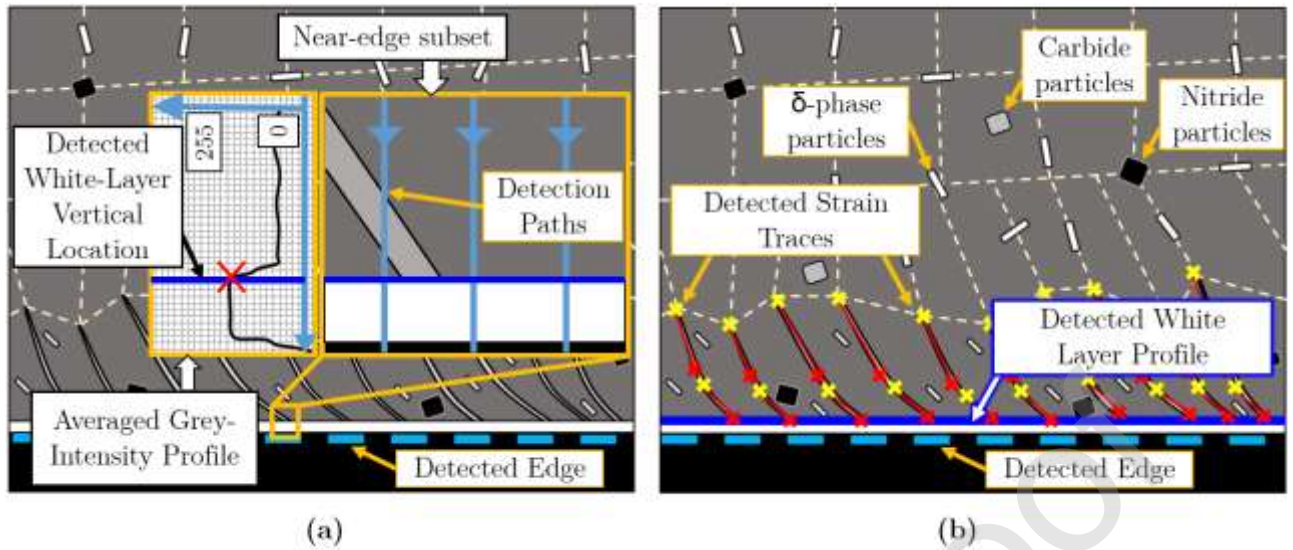

Figure 5 – White layer detection strategy. a) Subset generation and grayscale profile evaluation. b) Detected white layer.

Their height is a user-defined parameter, which should be conservatively chosen greater than the maximum white layer thickness expected. The algorithm firstly evaluates the grayscale intensity profile for each vertical line (column) of the digital subset (sub-matrix). A representative grayscale intensity profile is then calculated by averaging the previously stored vertical profiles. This signal represents the mean grayscale intensity distribution along the vertical direction for the considered subset. A peak in correspondence of the zone close to the sample edge is expected if the area under observation is affected by presence of white layer. In this way, the white layer extent can be evaluated detecting occurrence of peaking in the subset grayscale profiles in the vicinity of the edge, as shown in Figure 5 (a). Repeating this procedure for each near-edge subset, the white layer profile is obtained for the whole material area captured in the input micrograph, as shown in Figure 5 (b).

2.4 Automated processing of multiple micrographs

Because of the magnifications required to capture the microstructural features of interest, digital micrographs can only display a limited material region of the specimen under observation. On one hand, resolving features at relatively high magnification is desirable to have a convincing representation of the material condition investigated. Higher magnification also provides a higher pixel-to-μm ratio, which leads to a higher μm accuracy for a given pixel size when performing digital or manual measurements on a micrograph. However, for fixed pixel dimensions, increasing magnifications reduce the μm extension of the area under observation. Therefore, when large areas need to be investigated, higher magnifications can significantly increase the number of micrographs necessary to cover the desired region. Thus, the magnification employed for micrographs acquisition represents a trade-off between the quality of the input data, with possibility of clearly identify small-size features, and the acquisition and post-processing time consumption.
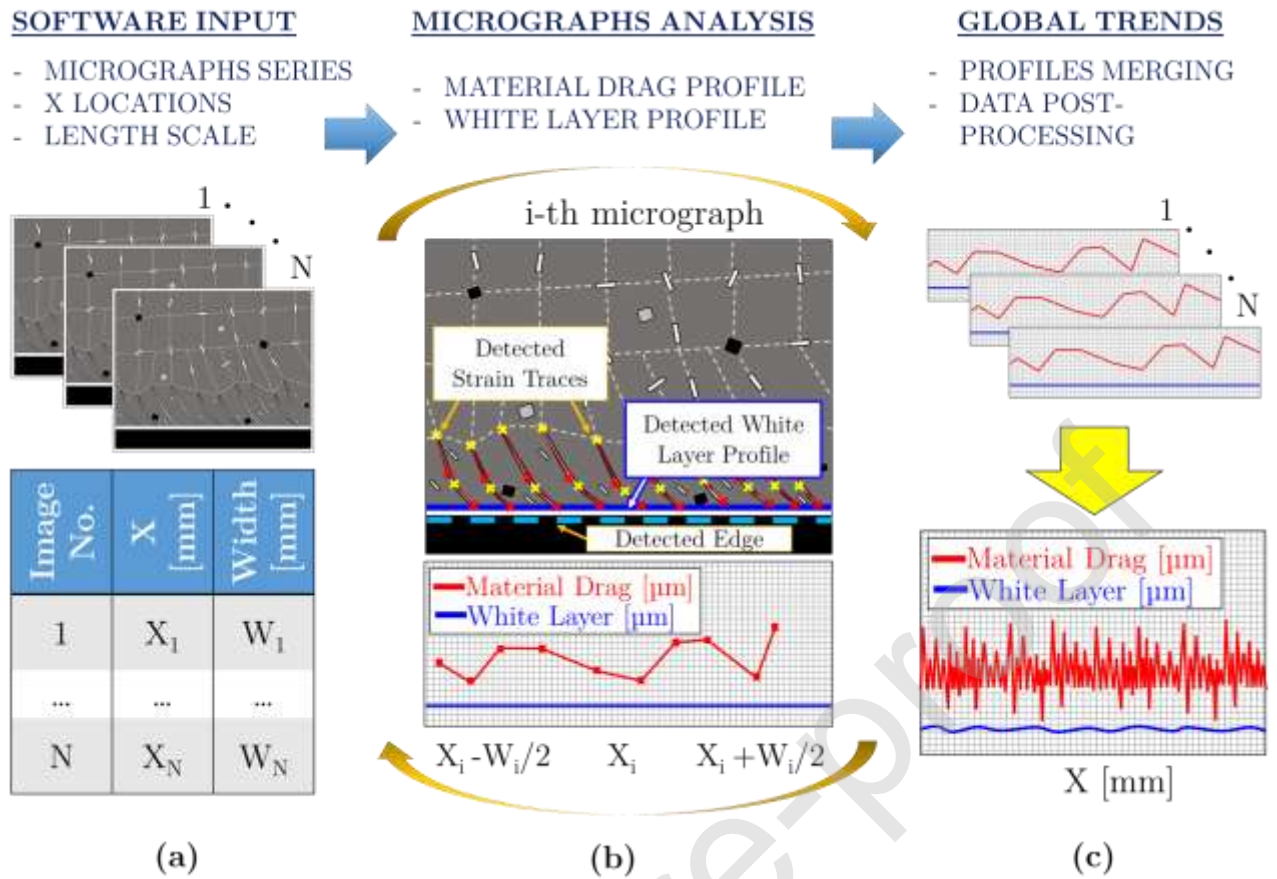
Figure 6 – Automated processing of multiple micrographs. a) Software input: digital images, locations and length scale. b) Cyclic surface integrity detection. c) Construction of global trends.

Nevertheless, the possibility of automating the measurement operation offers a significant advantage in this sense. To this aim, after the framework for processing a single micrograph has been developed, the algorithm has been upgraded in order to provide possibility of automatically processing a series (1-N) of micrographs. The logical route to reach this goal is presented in Figure 6. The inputs provided to the software include a directory path where the digital micrographs are stored, and a table where information on the location and scale unit of each micrograph is reported. In this context, the location of each micrograph is referred to a fixed point on the specimen, which is taken as origin of a one-dimensional horizontal reference system. This can be done simply storing the stage coordinates of the SEM machine for each captured image. The input file hence includes the X coordinate associated to each micrograph as relative distance of its centre from the reference location, as shown in Figure 6(a). In this way, the centre of each micrograph is referenced in a global frame. At this point, the X coordinate of each detected feature in the micrograph can be also referenced to the global coordinate system, once their X distance from the centre of the micrograph is known. This is a straightforward operation once the pixel-to-mm ratio of the image is known. Therefore, an additional column of the input file reports the image width of each micrograph in millimetres, W in Figure 6(a). This is used for the pixel-to-mm conversion that enables both global referencing of the detected features and dimensional measurement of their extent. Thus, after reading the input

file, the algorithm executes for each input micrograph the digital surface integrity assessment, as displayed in Figure 6(b).

At each iteration, the extent of each detected feature is assigned to its X location in the global reference system. Of course, a small overlapping between two consecutive micrographs is desirable, both to ensure complete covering of the area to be studied and to clearly capture features that might end up split between two consecutive images. From a numerical point of view, this might induce the presence of duplicated quantities in case features are detected close to the vertical borders of the micrograph. Therefore, a merging threshold is applied. This simply means that if the distance between two values in the detected profile is lower a given threshold, they are considered as the same item. Finally, once the N micrographs have been processed, the detected quantities can be plotted and eventually post-processed to analyse and interpret the information they contain.

3 Material and methods

Microstructural properties of a material depend both on its composition and on its processing route. Within the present work, the material selected for analysis is nickel-base superalloy Inconel 718 with grain size of 20-40 micrometres. In order to investigate the effect of process-induced plasticity on the material microstructure, machining specimens have been generated in orthogonal cutting conditions. The experiments have been carried out employing the Pendulum-Based Cutting Test (PBCT) machine presented by Xu et al. (2020). This approach namely enables a quick method for machinability and surface integrity assessment as a result of material removal. Cutting forces have been monitored through a Kistler 9275B dynamometer and NI 9223 data acquisition system. The cutting speed has been measured by recording and tracking the process with 4.5 kHz frame rate through a high-speed camera (IDT Y4). An informed description of this experimental procedure has been provided by Xu et al. (2019). In this way, surfaces were generated on Inconel 718 samples. Fresh cutting inserts of coated carbide grade (CP500 – Seco Tools) have been selected for the present tests with 0° rake angle and 50 μm edge rounding. In order to perform material analysis, the tested specimens have been embedded in conductive mounting compound and cross-sections with normal perpendicular to both the cutting direction and the machined surface has been obtained through gradual grinding and polishing steps, following common practice sample preparation procedures for nickel-base superalloys. Electrochemical etching was performed on the polished specimen surface with a 0.1 M solution of oxalic acid in water. Observation of the microstructural features in the proximity of the generated surfaces was carried out through field emission gun scanning electron microscopy (FEG-SEM) with JEOL machines models 7000F and 7100F. FEG-SEM micrographs have been acquired and employed to perform the automated detection algorithm in both Backscatter Electron (BSE) and Secondary Electron (SE) modes. Once the etched surface was observed and characterized through FEG-SEM, it has been re-polished in order to carry out EBSD mapping through a Nordlys Max 3 detector from Oxford Instruments, with typical step

sizes smaller than 100 nm. Resulting indexing accuracy is typically above 90%, where occurrence of unindexed points is mostly due to the presence of mounting resin (adjacent to the sample's edge) in the mapped area. Data analysis has been performed through the software Channel 5. In this way, isolated points recognised by the software as "wild spikes" have been removed from the map, and no other data filtering has been applied. This approach enabled comparison of the nanoscale crystallographic information extracted through EBSD with the microscale outputs obtained with the developed digital detection algorithm.

4 Results and Discussions

4.1 Material Drag: digital assessment

The proposed detection strategy for digital surface integrity characterisation has been applied to investigate the microstructural alterations generated in Inconel 718 as a result of material removal through chip formation. The strain-traces digital detectability strongly depends on the quality of the input data. It has been found that for this class of applications BSE imaging provided a preferable dataset quality that simplified the detection parameters optimization. It is remarked that being this method designed to automate the measurement process, it is essential to standardise the sample preparation and electron imaging strategy. This should be done by clearly defining mounting, polishing and etching parameters. Brightness, contrast and imaging mode should also be fixed in order to generate the input micrographs under constant conditions. Preferential imaging conditions depend both on the nature of the sample and on the detection target. Nevertheless, it is generally convenient to select them in such a way that the grayscale levels of the features of interest result distant from the ones of the surrounding background. In this way, the preferential contrast/brightness combination for digital detection was here selected to obtain a bright appearance of the features to be detected, against a darker aspect of the surrounding background. Once the working conditions and procedures have been optimised for a given application, employing a standardised framework allows minimising the calibration effort, as it will be discussed within the subsequent sections. Figure 7 (a) shows a representative BSE micrograph obtained through FEG-SEM, displaying microstructural indications of strain at shallow depths in the material subsurface. The pre-processing filter has been applied to the digital image in order to generate a suitable binary map to be used as input for the subsequent Hough-transform-based strain line detection. As a first step, pixels corresponding to delta-phase particles have been identified on a greyscale basis, taking advantage of the fact that their appearance is the brightest in the digital image. In this way, they could be successfully blackened, generating the digital data shown in Figure 7 (b). Evaluating local grayscale values and gradients in the resulting dataset, a binary strain traces map has been obtained. Hence, the candidate strain-traces pixels have been isolated, generating the binary matrix whose representation in the image space can be found in Figure 7 (c). Applying the Hough operator, elements of the image space are

15

transformed into points of the Hough-space. Evaluating the peaks of the so-obtained Hough-function in the Hough-space coordinates system (ρ, θ) plotted in Figure 7 (d), identification and detection of lines in the input dataset is performed and displayed in in Figure 7 (e). Figure 7 (f) shows the digitally detected strain-traces lines referenced to the original micrograph. Finally, sample edge detection has been carried out, as displayed in Figure 7 (e)-(f), enabling the estimation of the drag-affected layer profile reported in in Figure 7 (g). This is obtained by calculating the projected distance between the uppermost vertexes of each detected line (marked with yellow crosses in Figure 7 (e)-(f)) from the detected sample edge, completing digital assessment of the material drag extent for the selected micrograph. When comparing the outputs of the detection algorithm with the visual information observable in the input micrograph, an accurate correspondence between the detected lines and the strain traces is immediately recognised. Namely, the maximum obtained for the digitally assessed material drag profile in this site is 18.7 µm, which is very convincing when manually assessing material drag levels by visual observation of the same micrograph. In order to further investigate the microstructural condition of the generated subsurface, EBSD mapping has been performed on the same material site. Figure 7 (h) shows a detailed inverse pole figure (IPF) map revealing spatial distributions of crystallographic orientation in the material lattice in the vicinity of the machined edge of the specimen. Presence of severe grain refinement and fragmentation is observed in narrow material regions, exemplifying the profound microstructural reconfiguration occurred in the alloy as a result of the critical plastic conditions induced by the chip formation process. Moving away from the machined edge, the grain size fast increases while the microstructural condition exhibits an ever-less-distorted character over distances in the range of few micrometres, providing indication on the very local character of the plastic field generated in the workpiece. With reference to Figure 7 (f), it can be seen how the geometry of the digitally detected lines is coherent with the grain distortion appreciable through observation of the EBSD map shown in Figure 7 (h). Namely, the IPF map shows how the crystallographic orientation of the material lattice rapidly changes moving from shallow to higher depths in the sample sub-surface.
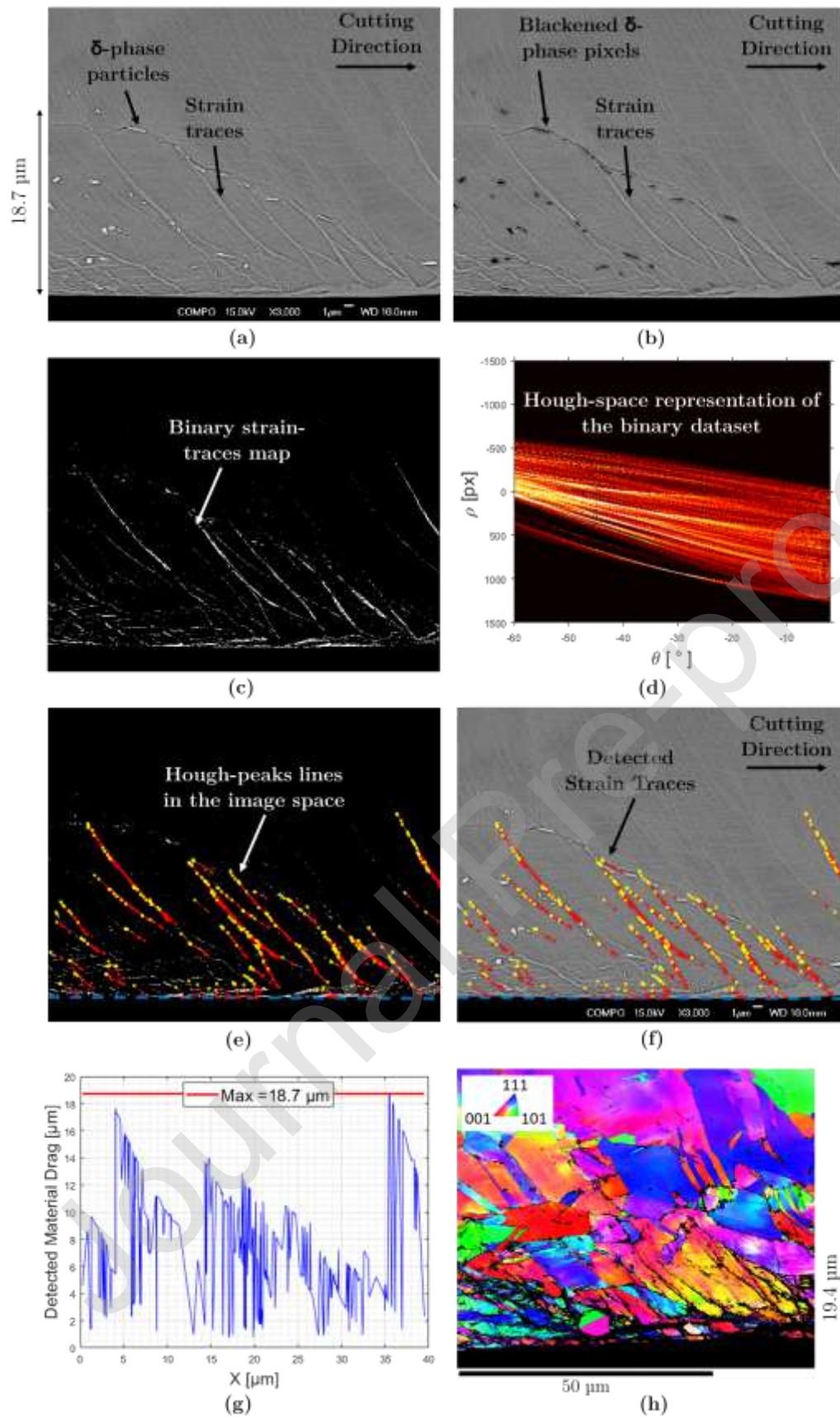
Figure 7 –BSE micrograph digital processing. a) Input micrograph. b) Delta-phase removal. c) Binary strain-traces map. d) Hough-space representation of the transformed binary dataset. e) Strain traces and edge detection. f) Strain traces and detected edge representation on the input micrograph. g) Detected material drag profile. h) EBSD map (IPF-Y) of the site under investigation. Cutting Speed= 78 m/min. Depth of Cut=100 μm.

17

The representation of such concentrated lattice distortion results in the visualization of relatively high differences in inter- and intra-granular orientation in the very proximity of the sample edge, forming on a greater scale a pattern of bended and fragmented grain regions. These anomalous microstructural features are very typical of advanced alloys subject to mechanical material removal. The highly detailed microstructural material state revealed through EBSD analysis is found to be geometrically coherent with the higher-level features identifiable by SEM imaging coupled with the present digital detection strategy. On one hand, a clear correspondence in terms of inclination and extent is found between the strain traces in the BSE micrograph in Figure 7 (a), and the shear-affected regions revealed in the IPF map in Figure 7 (h). Additionally, a correspondence is also obtained between the strain traces observed in Figure 7 (a), and the digitally detected lines shown in Figure 7 (e)-(f). Hence, a closed-loop relationship is found between the digital lines output of the present detection strategy, the strain traces observable by SEM imaging, and the lattice distortion obtained by EBSD indexing, resulting in comparable values for the drag-affected depth obtained employing such different strategies, as shown in Figure 7 (a)-(g)-(h). This is due to a substantial link between the strain traces observable through material etching and the microstructural condition of the volume under observation, together with an efficient development of the digital detection algorithm. An additional example of material drag resulting from mechanical material removal is represented in Figure 8. In this case, the observed area has been resolved through SE imaging. Differently from BSE ones, SE micrographs tend to display more topographical content from the observed surface. Although this might not represent a great difference for a human observer when recognising microstructural features, when it comes to the digital detection strategy, it introduces necessity of recalibrating the algorithm with a contextual detection parameter optimization. This mainly involves the pre-filtering section of the routine that generates the binary strain traces map representing the input domain where the Hough operator is applied. Namely, the presence of topographical information in the micrograph might introduce additional effort to digitally isolate the features of interest. Presence of accidental surficial contaminations on the specimen tends to not be observed when imaging in BSE mode, while it is more likely to be detected when SE imaging is employed. On the other hand, SE imaging normally offers a greater digital resolution, being this technique more surface-sensitive. Therefore, preliminary effort should be invested in understanding which set of sample preparation and imaging conditions is most effective for a specific application, as it has been done within the development of this procedure by investigating the digital processability of micrographs produced under different conditions. Nevertheless, in the present work, the digital approach was successfully applied to perform automated detection of strain-traces from SE micrographs. With reference to Figure 8 (a), the observed site displays limited levels of material drag, which from manual measurements appear to be in the range of 7 μm. Such micrograph, as an example among others, has been digitally inspected through the present algorithm, whose visual outputs have been reported in Figure 8 (b) in terms of detected strain lines and edge location. Also for this scenario, the algorithm was able to accurately measure the depth of the drag-affected area, returning a maximum of 7.1

μm for this material site. In-depth crystallographic information on this material site are additionally obtained through EBSD analysis.
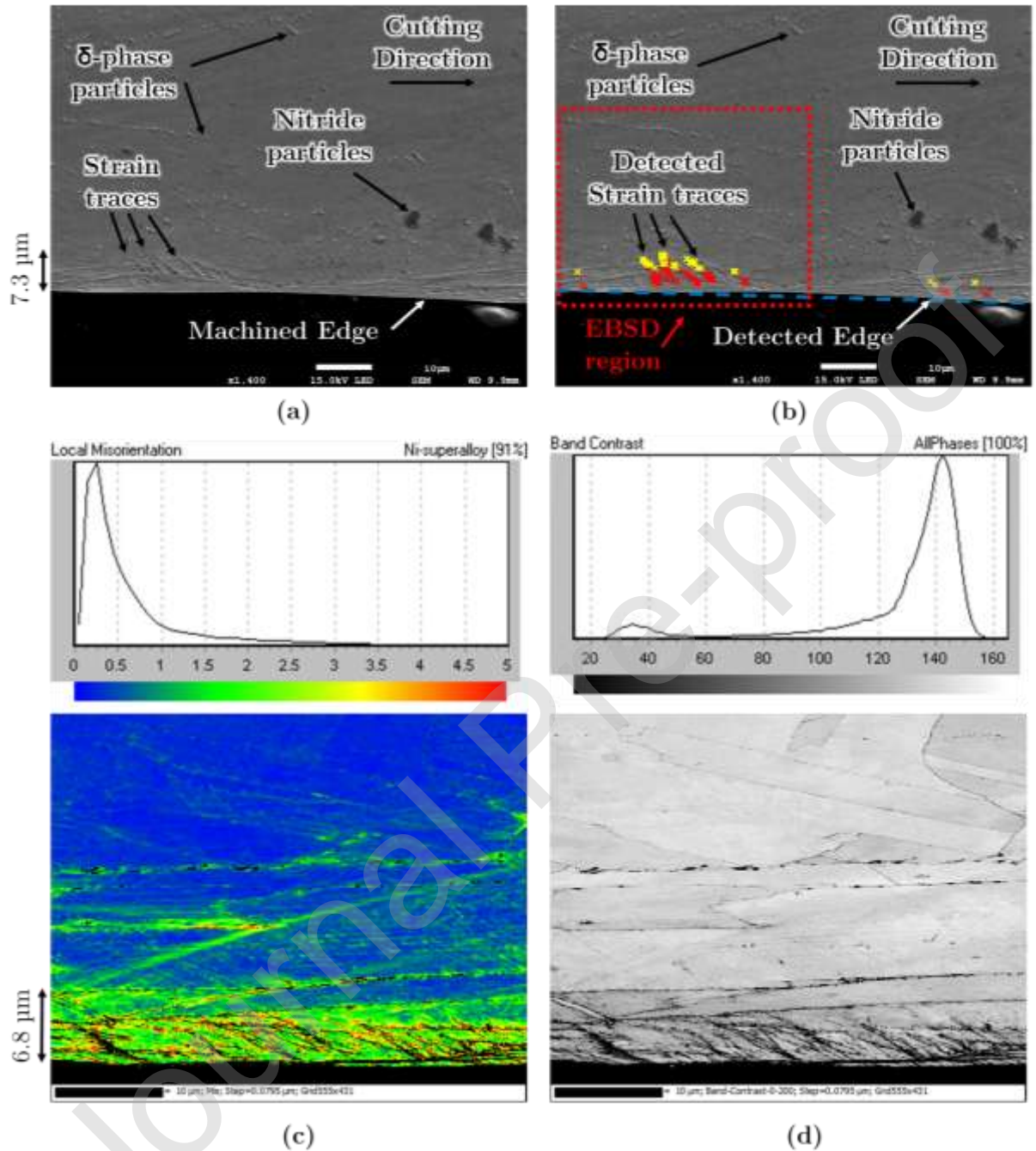

Figure 8 - SE micrograph digital processing. a) Input micrograph and EBSD mapping region. b) Strain traces and edge detection. c) EBSD map - Local Misorientation. d) EBSD map - Band Contrast. Cutting Speed=125 m/min. Depth of cut =70 μm.

High-detail quantitative information to survey the microstructural condition in the present site, and therefore verify the accuracy and validity of the proposed digital method, is obtained by mapping the spatial distribution of local lattice misorientation, as reported in Figure 8 (c). This map shows the difference in local crystal orientations

19

between neighbouring lattice sites within a grain, where a value of 10° has been selected for the evaluation of High-Angle Grain Boundaries (HAGBs), in consistence with previous approaches for this class of applications as reported by Brewer et al. (2006) and Schwartz et al. (2009). From the local misorientation histogram and legend in Figure 8 (c), it is found that the frequency peak for the mapped area lies at an angle smaller than 0.5°. In this map, highest levels of local misorientation are found in material areas near to the generated surface, decreasing when moving towards higher sub-surface depths. An arrow indicating a distance of ca. 7 µm is reported next to this map, showing consistency between the evaluation of the plastically affected depth obtained by lattice misorientation analysis, visual/manual micrograph inspection and digital detection strategy. To further survey the outcomes of the digital algorithm, additional information here employed to quantitatively evaluate the entity of the machining-induced subsurface microstructural alteration is obtained by analysis of Band Contrast (BC) EBSD maps. The BC map shown in Figure 8 (f) specifically provides information on the lattice condition in the site under investigation, quantifying the quality of the Electron Backscatter Patterns collected within the EBSD mapping process. More in detail, plastically affected regions and grain boundaries usually exhibit relatively low BC values because of the high lattice distortion typical of these areas. Such condition namely induces the backscattered electrons to diffract in a wide fan of directions, thus resulting in lower signal detected by the phosphoric screen of the EBSD camera with consequent lower EBSD pattern quality. This is one of the reasons why indexing material sites affected by high-levels of plastic deformation can be extremely challenging, usually requiring small mapping steps, which in the present case was about 80 nm for the analysis in Figure 8 (c)-(d) and ca. 60 nm for the map in Figure 7 (h). In this respect, it can be observed that, although the pattern quality and consequently the BC values are found to exhibit high levels for most of the points in the map in Figure 8 (d), low BC regions are concentrated at shallow depths in the material sub-surface, where peaks in the local misorientation values were previously found. Hence, it can be concluded that the lattice condition resulting by the analysis of this map is congruent with the previous evidence, being in close agreement with the quantitative interpretation of the material condition provided by EBSD misorientation analysis, visual micrograph inspection, and digital detection of material drag.

4.2 White layer: digital assessment

When metal cutting is performed under abusive conditions, traces of material drag can be accompanied by the undesirable generation of white layer attached to the new surface. Therefore, checking and evaluating the presence and eventual extent of white layer is an important task for many applications that involve the study of the microstructural response of advanced alloys to machining operations. When it comes to the present digital approach, the conceptual framework followed to design the white layer detection algorithm has been described in a schematic way in section 2.3. In the following, an application of this procedure to a BSE micrograph is discussed, in order to demonstrate how the developed digital algorithm permits computer-based inspection. With respect to previous cases, different observation conditions have been selected, such as lower accelerating voltage, lower magnification and a different

contrast/brightness combination. The input BSE micrograph under consideration is presented in Figure 9. Also in this case, since the employment of different SEM settings required a new optimization of the detection parameters. Figure 9 (a) shows the whole input image, from which near-edge subsets have been obtained, as the one magnified in Figure 9 (d). In order to determine the subset location, the edge location had been previously detected. The subset height (SH) selected for the present case is 3.5 µm. This parameter should be conservatively chosen greater than the maximum white layer thickness expected.
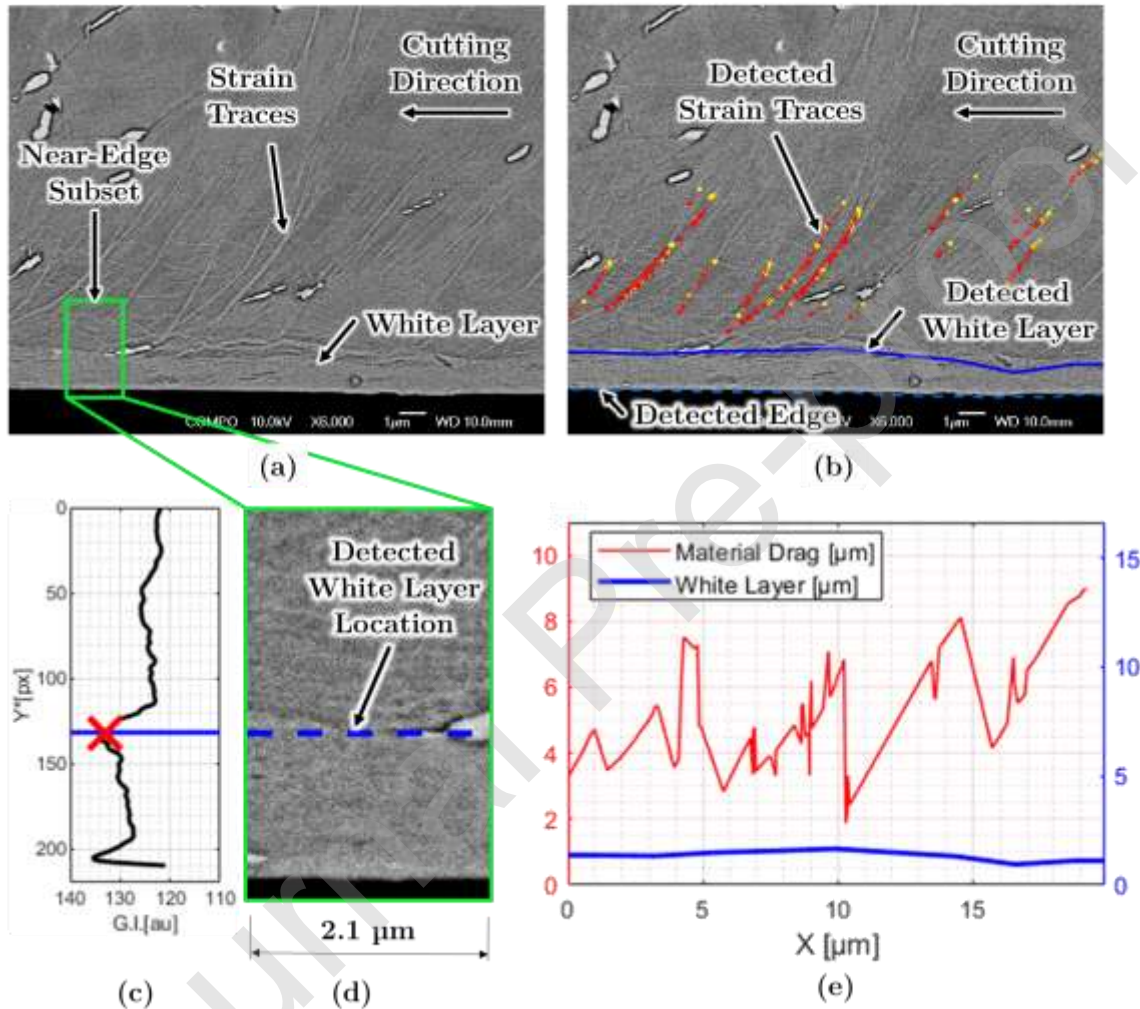

Figure 9 –Input SE micrograph with single near-edge subset detail location a). Detected features represented on the input micrograph: Strain traces, White Layer and Sample Edge b). Grayscale intensity profile generation for the selected near-edge subset c). Near-edge subset magnified view with detected white layer location d). Material Drag (red) and White Layer (blue) profiles generated for the input image (e). Cutting Speed=65 m/min. Depth of cut =150 µm.

The correctness of this value can be later verified checking that the detected white layer thickness is lower than the SH selected. The rectangular subset width is adaptively defined proportionally to the SH, which in this case resulted into a subset width of 2.1 µm. For each of the subsets, the representative greyscale profile has been obtained as explained in section 2.3, enabling the detection of the white layer at the discretized

horizontal locations in which the micrograph was divided. Figure 9 (c) shows the actual representative greyscale profile obtained for the subset under consideration, reporting with a red cross and a blue line the vertical white layer location resulting from the digital analysis. For each subset, presence and thickness of white layer is detected by evaluating existence and eventual extent of peaking zones in the averaged subset grey-intensity profile. Iterating this procedure for each subset generated along the sample edge (X-axis), the full output is obtained and visually represented in Figure 9 (b), where a solid blue line shows the detected white layer on the input BSE micrograph, together with the detected strain lines and sample edge. The resulting digitally detected surface integrity is quantitatively reported in Figure 9 (e), in terms of white layer thickness and the material drag depth as a function of the horizontal coordinate. Although the white layer object of detection can be clearly visualized by the human eye in the micrograph, its extension is quite small compared with the image dimensions. A curios human observer might be tempted to employ higher magnifications to study this material site more in detail, with possibility of advanced interpretation. However, when it comes to the present computing algorithm, the main output of interest is the measurement of the white layer thickness. Therefore, the size of the material site captured in a single micrograph should be chosen small enough to enable correct detection, but as large as possible to maximize the area inspected in a single step. Moreover, the magnification choice in this case was also influenced by the necessity of having an image capturing the vertical extent of the strain traces and unaffected material in this site. Another important remark is that the optimal SEM conditions for white layer detection might be different from the ones that enhance the digital representation of the strain traces in the image. Therefore, when mapping large areas, conditions representing the best compromise need to be identified. Nevertheless, it can be clearly appreciated that for the present case the algorithm successfully detected both white layer thickness and material drag depth present in the input micrograph.

4.3 Digital Surface Integrity assessment: automated analysis of large material regions

Development of digital detection procedures for surface integrity assessment introduces the possibility of evaluating the machining-induced material condition under fixed inspection parameters. For what concerns the discussion carried out in the previous paragraphs, the analyses presented were focused on specific material sites displaying local microstructural conditions. A complementary strategy was implemented for serial processing of multiple digital inputs, to demonstrate the applicability of the approach to map areas having extensions that require acquisition of multiple micrograph for their observation. To this aim, a series of micrographs has been collected through FEG-SEM under constant imaging conditions. Sequentially moving the SEM stage about its X-axis with increments of 100 µm, a total of 40 micrographs with 108.75 µm width has been digitally acquired, resulting in an 8.75% overlapping length for each frame. The present algorithm has been hence applied to map the material condition resulting in a machined specimen over a total length of 4 mm. In this context, the digital algorithm processed each micrograph under constant

pre-fixed conditions. Although this enables process automation, it also requires all the micrographs to be digitally inspected under the same detection settings. In this case, since the algorithm works with numerically fixed parameters, features appearing very similar to the human eye might exhibit different detectability, both because of eventual imperceptible modifications in the local pixel colour map, or because of the nature of the algorithm itself. Therefore, to successfully carry out this operation, the detection strategy had to be optimised on a global basis.
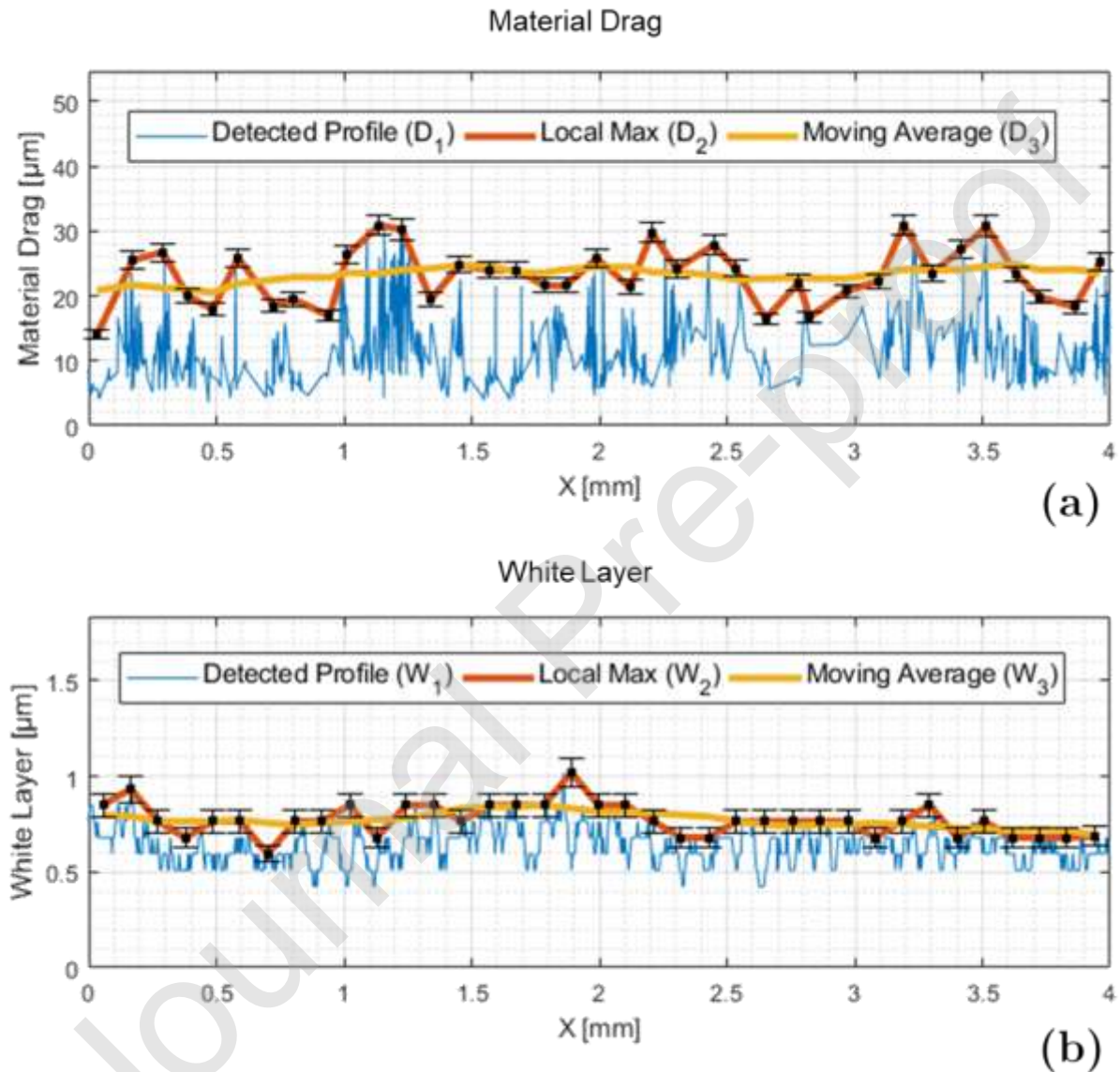

Figure 10 – Digital detection applied on large areas. An example of Inspection of 4 mm cutting length using with multiple micrographs of 100 μm width. (a) Material Drag output: rough profile as detected 'D1', local maxima 'D2', moving average of local maxima 'D3'. (b) White layer output: rough profile as detected 'W1', local maxima 'W2', moving average of local maxima 'W3'. Depth of Cut=60 μm. Cutting Speed 120 m/min. Specific cutting forces K_Y = 3.8 kN/mm², K_Z=5.1 kN/mm².

To support the identification of suitable settings for this specimen and imaging condition, the measurement error has been estimated comparing the digital output to

manual measurements for micrographs taken every 0.5 mm distance, both for the detected white layer and material drag extent. On this basis, a linear calibration function has been introduced and applied to correct the measurement output, as it is done for conventional measurement instruments. The outputs resulting for the Material Drag and White Layer have been presented in Figure 10 (a) and (b), respectively. The rough "as detected" profiles have been reported in Figure 10 (a)-(b), along the whole length mapped, both for the Material Drag and White Layer, and respectively indicated as 'D_1' and 'W_1'. These profiles are generated merging the profiles obtained for each individual micrograph digitally analysed, as explained in section 2.4. Therefore, 'D_1' reports the extent of each strain line detected in each input micrograph, referencing its extent to the corresponding X location in the global frame of reference. It is clear from the previously displayed micrographs that presence of strain traces does not occur continuously. In each of the previously analysed cases, it can be noticed that the length and occurrence of these features has a non-constant character. In a limit case, employing a magnification high enough, a single SEM micrograph could potentially be produced with no visible indication of strain, lacking information on the material condition in that particular site, which would instead need to be surveyed with more in-depth approaches such as EBSD indexing. Nevertheless, it has been previously demonstrated that for the scales of observations of practical interest, a very close correlation between the maximum deformation revealed through EBSD analysis and the maximum material drag observed by SEM imaging – and hence digitally detectable – existed. Against this background, to obtain a meaningful measurement of the material deformation, the local maxima of the 'as detected' profile D_1 has been calculated over X intervals of adequate width. This has been performed with an interval size of 100 μm, plotting the resulting data as 'D_2' Figure 10 (a). In other words, this means that for each analysed micrograph, the attention is not focussed anymore on the detail of each detected line, but on the local maximum instead, representing this value the relevant measurement of the deformation level present in that material site. The same approach has been followed for post-processing the 'as detected' white layer profile, resulting in the curve 'W_2' in Figure 10 (b). Together with curves 'D_2' and 'W_2', error-bars indicating the residual measurement error after calibration is shown. The calibration procedure was also undertaken following a similar logic, which involved manual evaluation of the maximum drag and white layer extent in equally spaced micrographs, whose values have been cross-checked against the outputs of the digital tool. Finally, the trend lines 'D_3' and 'W_3' have been obtained as moving average of 'D_2' and 'W_2' over a moving length of 1 mm. In this way, this logical flow enabled to: (i) punctually check each anomaly detectable in the micrographs, (ii) obtain a meaningful maximum value for each inspected site, and (iii) produce a representative average value that takes into account of the spatial variability of the available signal. This indicates possibility for the digitally detected trends to be collated to relevant macroscopic process conditions, such as cutting speeds and forces, broadening the process understanding and making digital data available from a surface integrity perspective.

5 Conclusions

Controlling the microstructural surface integrity of machined components is a fundamental task when processing advanced materials for high-value safety-critical applications. However, the assessment of microstructural surface integrity levels still strongly relies on manual measurements involving repetitive procedures, which might be affected by lower repeatability if compared with computer-based routines. In this work, a digital approach has been realised, to leave to a machine the task of inspecting micrographs representing the microstructural conditions of interest. In particular:

- The conceptual flow that enabled implementation of the digital surface integrity assessment algorithms has been presented. The logical structure behind the techniques adopted to carry out computer-assisted inspection of digital micrographs has been outlined, clarifying the logic approach followed to design algorithms capable of digitally recognising presence and extent of machining-induced material drag in relevant specimens. This has been subsequently extended and integrated with an additional routine performing white layer detection, whose working principle has been discussed as well.

- Different scenarios have been taken into consideration, showing the possibility of applying such strategy to micrographs exhibiting different level of deformation and acquired under different imaging conditions. The algorithm namely succeeded in detecting higher material drag levels, in the range of 19 μm, as well as lower indications of deformation, in the range of 7 μm, which can result more difficult to judge on a visual basis. In addition, possibility of digitally processing both SE and BSE micrographs has been demonstrated. As a result, a convincing correspondence between the digitally detected features and the visually-appreciable information has been found.

- High-detail FEG-SEM observation coupled with EBSD orientation mapping enabled in-depth analysis of the workpiece subsurface microstructural integrity. Fine-step EBSD indexing has been namely undertaken with step sizes in the range of 80-60 nm. In this way, in-depth information on the microstructural material state was obtained by analysis of IPF, BC and misorientation maps. This approach was essential to investigate the fundamental small-scale material phenomena involved within the thermo-mechanically complex processing conditions that develop when machining high-temperature alloys. Furthermore, it provided a meaningful comparative understanding of the link existing between the outputs of different techniques applied to the observation of same material conditions. As a result, a close-loop relationship has been found between the levels of deformation manually evaluated on SEM micrographs, the ones digitally detected, and the interpretation of the corresponding EBSD outputs. This represented a key step within the development of the present algorithm, to survey its applicability and collocation.

- On the other hand, because of their elevate processing time and local character, in-depth material analyses such as the one previously discussed are mostly effective to study with a high level of detail only limited material portions. Nevertheless, when surface integrity of large material sites needs to be assessed, the present digital approach has been demonstrated to be applicable. Digital surface integrity has successfully been detected over a cutting length of 4 mm with micrographs spacing of 100 μm and an overlapping of 8.75 %. White layer and material drag levels have been detected from micrographs acquired under constant imaging conditions and processed with fixed detection parameters. Measurement calibration has been undertaken against sample measurements manually evaluated, resulting in residual measurement errors for the calibrated digital instrument lower than 5%. Finally, the detected trends have been processed and stored, with possibility of collating macroscopic data available from conventional process monitoring approaches.

Possibility of digitally performing surface integrity assessment has been demonstrated and applied to the analysis of Inconel 718 specimens, representing this material a reference for nickel-base superalloys. Nevertheless, a possible route of advancement can be represented by the application of these concepts to different material systems, opening to the possibility of developing material libraries digitally available for automated surface integrity analysis. It is remarked that, given the character of this approach, different strategies for data manipulation, storage or future reprocessing could be implemented. This introduces the possibility of having available digital information that could potentially assist subsequent digital root-cause analyses and quality checks within production, or support the scientific understanding of researchers dealing with the study of process-induced material modification. To benefit the most from the automation, optimal sample preparation procedures and imaging conditions are to be identified and standardised for a given application, to minimise the parameter optimization and calibration effort required. What has been here presented is just one of the possible ways of processing the output data, which has been judged appropriate to interpret the detected material condition, enabling at the same time explanation of the conceptual scheme on which the algorithm relies. It is understood that, for each specific application, the advice and guidance of a specialist is mandatory to indicate appropriate data analysis and detection parameters, based on the knowledge and experience matured on the specific material and manufacturing process involved. The introduction of novel approaches must be namely based on and take maximum advantage of the existing experience, to guarantee consistency and awareness at all stages of the development process.

CRediT author statement

Andrea la Monaca: Conceptualization, Methodology, Software, Investigation, Validation, Formal analysis, Data Curation, Writing - Original Draft. **Zhirong Liao:** Methodology, Investigation, Validation, Formal analysis, Supervision. **Dragos Axinte:** Conceptualization, Investigation, Formal analysis, Writing - Review & Editing, Supervision

Declaration of interests

6 Acknowledgments

7 Data Availability

The raw/processed data required to reproduce these findings cannot be shared at this time as the data also forms part of an ongoing study.

References

Adams, B.L., Wright, S.I., Kunze, K., 1993. Orientation imaging: The emergence of a new microscopy. Metall. Trans. A 24, 819–831. https://doi.org/10.1007/BF02656503

Arunachalam, R.M., Mannan, M.A., Spowage, A.C., 2004. Residual stress and surface roughness when facing age hardened Inconel 718 with CBN and ceramic cutting tools. Int. J. Mach. Tools Manuf. 44, 879–887. https://doi.org/10.1016/j.ijmachtools.2004.02.016

Bock, R.K., Gheorghe, A., Krischer, W., Levinson, L., Natkaniec, Z., 1995. A commercial image processing system considered for triggering in future LHC experiments. Nucl. Inst. Methods Phys. Res. A. https://doi.org/10.1016/0168-9002(94)01396-9

Brewer, L.N., Othon, M.A., Gao, Y., Hazel, B.T., Buttrill, W.H., Zhong, Z., 2006. Comparison of diffraction methods for measurement of surface damage in superalloys. J. Mater. Res. 21, 1775–1781. https://doi.org/10.1557/jmr.2006.0199

Campbell, A., Murray, P., Yakushina, E., Marshall, S., Ion, W., 2018. New methods for automatic quantification of microstructural features using digital image

processing. Mater. Des. 141, 395–406. https://doi.org/10.1016/j.matdes.2017.12.049

Collins, P.C., Welk, B., Searles, T., Tiley, J., Russ, J.C., Fraser, H.L., 2009. Development of methods for the quantification of microstructural features in α + β-processed α/β titanium alloys. Mater. Sci. Eng. A 508, 174–182. https://doi.org/10.1016/j.msea.2008.12.038

Connolley, T., Starink, M.J., Reed, P.A.S., 2004. Effect of Broaching on High-Temperature Fatigue Behavior in Notched Specimens of INCONEL 718. Metall. Mater. Trans. A Phys. Metall. Mater. Sci. 35 A, 771–783. https://doi.org/10.1007/s11661-004-0005-z

Davim, J.P., Rubio, J.C., Abrao, A.M., 2007. A novel approach based on digital image analysis to evaluate the delamination factor after drilling composite laminates. Compos. Sci. Technol. https://doi.org/10.1016/j.compscitech.2006.10.009

Gavalda Diaz, O., Garcia Luna, G., Liao, Z., Axinte, D., 2019. The new challenges of machining Ceramic Matrix Composites (CMCs): Review of surface integrity. Int. J. Mach. Tools Manuf. 139, 24–36. https://doi.org/10.1016/j.ijmachtools.2019.01.003

Gillibert, L., Jeulin, D., 2013. 3D Reconstruction and analysis of the fragmented grains in a composite material. Image Anal. Stereol. 32, 107–115. https://doi.org/10.5566/ias.v32.p107-115

Gonzalez, R.C., Woods, R.E., Eddins, S.L., 2010. Digital Image Processing Using Matlab, 2nd Editio. ed. McGraw Hill.

Hardy, M.C., Herbert, C.R.J., Kwong, J., Li, W., Axinte, D.A., Sharman, A.R.C., Encinas-Oropesa, A., Withers, P.J., 2014. Characterising the integrity of machined surfaces in a powder nickel alloy used in aircraft engines. Procedia CIRP 13, 411–416. https://doi.org/10.1016/j.procir.2014.04.070

Herbert, C., Axinte, D., Hardy, M., Brown, P.D., 2012. Investigation into the characteristics of white layers produced in a nickel-based superalloy from drilling operations. Mach. Sci. Technol. 16, 40–52. https://doi.org/10.1080/10910344.2012.648520

Herbert, C., Axinte, D.A., Hardy, M., Withers, P., 2014. Influence of surface anomalies following hole making operations on the fatigue performance for a nickel-based superalloy. J. Manuf. Sci. Eng. Trans. ASME 136, 1–9. https://doi.org/10.1115/1.4027619

Hosemann, P., Frazer, D., Fratoni, M., Bolind, A., Ashby, M.F., 2018. Materials selection for nuclear applications: Challenges and opportunities. Scr. Mater. 143, 181–187. https://doi.org/10.1016/j.scriptamat.2017.04.027

Kappmeyer, G., Hubig, C., Hardy, M., Witty, M., Busch, M., 2012. Modern machining of advanced aerospace alloys-Enabler for quality and performance. Procedia CIRP 1, 28–43. https://doi.org/10.1016/j.procir.2012.04.005

Liao, Z., Abdelhafeez, A., Li, H., Yang, Y., Diaz, O.G., Axinte, D., 2019a. State-of-the-art of surface integrity in machining of metal matrix composites. Int. J. Mach. Tools Manuf. https://doi.org/10.1016/j.ijmachtools.2019.05.006

Liao, Z., Axinte, D., Mieszala, M., M'Saoubi, R., Michler, J., Hardy, M., 2018. On the influence of gamma prime upon machining of advanced nickel based superalloy. CIRP Ann. 67, 109–112. https://doi.org/10.1016/j.cirp.2018.03.021

Liao, Z., Polyakov, M., Diaz, O.G., Axinte, D., Mohanty, G., Maeder, X., Michler, J., Hardy, M., 2019b. Grain refinement mechanism of nickel-based superalloy by severe plastic deformation - Mechanical machining case. Acta Mater. 180, 2–14. https://doi.org/10.1016/j.actamat.2019.08.059

Lu, W., Wilson, R.S., Yang, L., Dun, A., Smyth, A.M., Duncan, R.R., Rickman, C., 2016. Automated single particle detection and tracking for large microscopy datasets. R. Soc. Open Sci. 3. https://doi.org/10.1098/rsos.160225

M'Saoubi;, R., Outeiro, J.C., Chandrasekaran, H., Jawahir, I.S., Jr., O.W.D., 2015. A review of surface integrity in machining and its impact on functional performance and life of machined products. Int. J. Sustain. Manuf. 1, 203. https://doi.org/10.1504/ijsm.2008.019234

M'Saoubi, R., Axinte, D., Herbert, C., Hardy, M., Salmon, P., 2014. Surface integrity of nickel-based alloys subjected to severe plastic deformation by abusive drilling. CIRP Ann. - Manuf. Technol. 63, 61–64. https://doi.org/10.1016/j.cirp.2014.03.067

Novovic, D., Dewes, R.C., Aspinwall, D.K., Voice, W., Bowen, P., 2004. The effect of machined topography and integrity on fatigue life. Int. J. Mach. Tools Manuf. https://doi.org/10.1016/j.ijmachtools.2003.10.018

Peregrina-Barreto, H., Terol-Villalobos, I.R., Rangel-Magdaleno, J.J., Herrera-Navarro, A.M., Morales-Hernández, L.A., Manríquez-Guerrero, F., 2013. Automatic grain size determination in microstructures using image processing. Meas. J. Int. Meas. Confed. 46, 249–258. https://doi.org/10.1016/j.measurement.2012.06.012

Sajedian, I., Kim, J., Rho, J., 2019. Finding the optical properties of plasmonic structures by image processing using a combination of convolutional neural networks and recurrent neural networks. Microsystems Nanoeng. 5, 27. https://doi.org/10.1038/s41378-019-0069-y

Schwartz, A.J., Kumar, M., Adams, B.L., Field, D.., 2009. Electron Backscatter Diffraction in Materials Science, Second. ed, Springer. New York, NY.

Shang, Z., Liao, Z., Sarasua, J.A., Billingham, J., Axinte, D., 2019. On modelling of laser assisted machining: Forward and inverse problems for heat placement control. Int. J. Mach. Tools Manuf. https://doi.org/10.1016/j.ijmachtools.2018.12.001

Singh, A.K., Kumar, B., Jha, K., Astarita, A., Squillace, A., Franchitti, S., Arora, A., 2020. Friction stir welding of additively manufactured Ti-6Al-4V: Microstructure and mechanical properties. J. Mater. Process. Technol. 277, 116433. https://doi.org/10.1016/j.jmatprotec.2019.116433

Thakur, A., Gangopadhyay, S., 2016. State-of-the-art in surface integrity in machining of nickel-based super alloys. Int. J. Mach. Tools Manuf. 100, 25–54. https://doi.org/10.1016/j.ijmachtools.2015.10.001

Wusatowska-Sarnek, A.M., Dubiel, B., Czyrska-Filemonowicz, A., Bhowal, P.R., Ben

Salah, N., Klemberg-Sapieha, J.E., 2011. Microstructural characterization of the white etching layer in nickel-based superalloy. Metall. Mater. Trans. A Phys. Metall. Mater. Sci. 42, 3813–3825. https://doi.org/10.1007/s11661-011-0779-8

Xu, D., Liao, Z., Axinte, D., Hardy, M., 2020. A novel method to continuously map the surface integrity and cutting mechanism transition in various cutting conditions. Int. J. Mach. Tools Manuf. 151, 103529. https://doi.org/10.1016/j.ijmachtools.2020.103529

Xu, D., Liao, Z., Axinte, D., Hardy, M., M'Saoubi, R., 2019. A quick method for evaluating the thresholds of workpiece surface damage in machining. CIRP Ann. 4–7. https://doi.org/10.1016/j.cirp.2019.03.015

Yang, D., Liu, Z., 2016. Quantification of Microstructural Features and Prediction of Mechanical Properties of a Dual-Phase Ti-6Al-4V Alloy. Materials (Basel). 9, 1–14. https://doi.org/10.3390/ma9080628

Zhang, H., Shen, X., Bo, A., Li, Y., Zhan, H., Gu, Y., 2017. A multiscale evaluation of the surface integrity in boring trepanning association deep hole drilling. Int. J. Mach. Tools Manuf. 123, 48–56. https://doi.org/10.1016/j.ijmachtools.2017.07.005

Zhang, X., Chen, Y., Hu, J., 2018. Recent advances in the development of aerospace materials. Prog. Aerosp. Sci. 97, 22–34. https://doi.org/10.1016/j.paerosci.2018.01.001

Zhang, Y., Guo, S., Zhang, Z., Huang, H., Li, W., Zhang, G., Huang, Y., 2019. Simulation and experimental investigations of complex thermal deformation behavior of wire electrical discharge machining of the thin-walled component of Inconel 718. J. Mater. Process. Technol. 270, 306–322. https://doi.org/10.1016/j.jmatprotec.2019.02.020

Zhao, Y.J., Liang, D.T., Song, K.C., Yan, Y.H., Li, H.N., 2019. Automatic measurement of grinding-induced white layer in titanium alloys based on image processing technique. Int. J. Adv. Manuf. Technol. https://doi.org/10.1007/s00170-019-04390-x

Zhou, J.M., Bushlya, V., Stahl, J.E., 2012. An investigation of surface damage in the high speed turning of Inconel 718 with use of whisker reinforced ceramic tools. J. Mater. Process. Technol. 212, 372–384. https://doi.org/10.1016/j.jmatprotec.2011.09.022